euronoise 2021
25th to 27th of October
Madeira, Portugal - online

Weakly Nonlinear Pulse Propagation in Large Caliber Weapons: a Time-Domain Approach based on the Nonlinear Progressive Wave Equation

Guido Billot[1], Benoît G. Marinus[1], Kristof Harri[1]

[1]Royal Military Academy, Department of Mechanical Engineering
{Guido.Billot@mil.be, Benoit.Marinus@mil.be, Kristof.Harri@mil.be }

Abstract

The propagation of high intensity impulsive noise poses challenges for the assessment of noise exposure for personnel and communities. Large pressure perturbations give rise to shock formation, enhanced energy dissipation and frequency content redistribution thereby ruling out the possibility to linearize the propagation equations. Common approaches involve computationally demanding frequency-domain solvers. The proposed algorithm solves the Nonlinear Progressive Wave Equation (NPE) with a time marching scheme that exploits a moving window coordinate frame and operator splitting technique. A Flux Corrected Transport scheme provides second-order accuracy for the nonlinear term and well-documented shock capturing capabilities. The observation of weakly non-linear waves during an on-site test campaign with a large caliber weapon offered the opportunity to compare the NPE and a linear solver, to gain scientific insight into the propagation of these pulses. Different sound exposure metrics are evaluated at various locations down the propagation line for benchmarking and the intrinsic limitations of the most pertinent standards are discussed.

Keywords: NPE, nonlinear, acoustics, propagation, FCT.

1 Introduction

Large-calibre weapons release a vast amount of acoustic energy within a time interval of few milliseconds, causing hazard for the auditory apparatus of the involved personnel and annoyance to nearby residential communities. Optimal mitigations (e.g. noise absorption barriers) and corrective measures can only be adopted after accurately modelling the Weakly Nonlinear Pulse Propagation in its complexity.

The challenge has been historically addressed with standards (ISO17201 [1], ISO9613 [2], Nordtest [3]) and in-house numerical propagation algorithms, but the lack of a comprehensive assessment framework is what motivates the present work. *Leissing* [4] and *Young et al.* [5] contributed by conducting studies on the propagation of explosion-originated blast waves, whereas examples of underwater propagation of strongly nonlinear shockwaves are also extensively documented ([6], [7]). One of the most acknowledged formulations of the nonlinear wave equation is the Khokhlov–Zabolotskaya–Kuznetsov equation, usually solved in the frequency domain. Aside of the computational burden, this spectral method is limited to narrowband frequency signals [8], typically ultrasonic beams with strong diffraction phenomena [9]. The Nonlinear Progressive Equation [10] illustrated here embeds in its time-domain formulation the capability to handle nonlinear broadband sources, provided the spatial discretization is carefully determined. The flexibility of the operator splitting approach introduces modularity in the algorithm and the Flux Corrected Transport scheme is designed

to preserve positivity and limit the numerical diffusivity when solving for large discontinuities such as shocks [11] . The solver is developed for the 1D formulation of the NPE equation, including atmospheric dissipation, refraction, nonlinearity and spatially varying sound speed.
Sec.2 contains a concise overview of the range of validity of the NPE equation and its structure. Sec.3 explains the choices made in the numerical implementation and is concluded by the validation of the results against an analytical solution. In Sec. 4, the equipment used in the measurement campaign is illustrated. Sec. 5 is devoted to the presentation and discussion of the results obtained, whereas in Sec. 6 the conclusions are drawn and directions for the continuation of this research are outlined.

2 Theoretical background

Acoustics boils down to the study of the pressure perturbation propagating in a medium with respect to the unperturbed ambient state. Whenever this deviation from the initial state exceeds a certain magnitude, the phenomena occurring can only be described by a nonlinear mathematical model. Shock formation, nonlinear steepening, harmonic redistribution, shock coalescence and enhanced energy dissipation are the main processes described in literature for nonlinear propagation ([5], [6], [7], [8]). There is no unique consensus on the precise value that marks the onset of nonlinearities. Values of 154 [dB re 20 μPa] and 130 [dB re 20 μPa] are often regarded as a reference ([1] , [3]). The nature of the logarithmic scale makes the dividing line even more ambiguous, as it corresponds to an interval ranging from 1000 [Pa] to 70 [Pa].

McDonald et al. [10] developed the original formulation of the Nonlinear Progressive Wave equation to study underwater high-intensity acoustic phenomena known as caustics. Its validity is restricted to weakly nonlinear perturbations travelling along a principal direction in a quiescent medium. The sound speed is allowed to fluctuate of a quantity c' from the ambient value c_0, so that the effective sound speed is $c = c_0 + c'$. These variations must be limited throughout the entire propagation ($c' << c_0$). Although extended formulations are available [12], the canonical form of the NPE can only accurately resolve shockwaves within 10° from the main propagation direction. For the complete derivation of the equation, the reader should refer to the original publications ([13], [14]). If only the one-dimensional terms are retained, the NPE simplifies to Eq. (1), where R is the dimensionless acoustic pressure:

$$\partial_t R = -\partial_x \left[c'R + \frac{\beta c_0 R^2}{2} \right] + \frac{\delta_{th}}{2} \partial_x^2 R \tag{1}$$

with

$$R = \frac{\rho'}{\rho_0} \approx p' / \left(\rho_0 c_0^2 \right)$$

Primed variables (ρ', p', c') indicate the state of perturbation with respect to the initial undisturbed condition (ρ_0, p_0, c_0). The first linear term on the right side member accounts for refraction and is responsible for the travelling of the waveform *within* the moving window. The second term includes nonlinearities and the third term represents atmospheric absorption. As a consequence of a coordinate transformation, the computational window moves forward along the direction x with the constant ambient state speed of sound c_0.
High intensity pressure perturbations affect the speed of the moving waveform in such a way that a distortion occurs:

$$c = c_o + c' \approx c_o + \left(\frac{\partial c}{\partial p} \right)_o p' \approx c_o + \beta v \approx c_o + \frac{\beta p'}{\rho_o c_o} \tag{2}$$

This first order expansion [15], where v is the wave particle velocity of a plane wave, introduces a direct proportionality between the acoustic pressure and the real speed of sound, yielding different portions of the waveform to travel with spatially varying speed. The coefficient of nonlinearity for air is $\beta = \frac{1+\gamma}{2} = 1.2$.

Atmospheric absorption includes two dissipation mechanisms: thermoviscous and relaxation losses. The first phenomenon is dominant, and will be the only one included in equation (1) through:

$$\delta_{th} = \frac{\left[\eta + \frac{4}{3}\mu + \kappa\left(\frac{1}{C_v} - \frac{1}{C_p}\right)\right]}{\rho_0} \tag{3}$$

Sound diffusivity encloses the thermophysical effects of the bulk viscosity (η), the shear viscosity (μ), the thermal conductivity (κ) and the specific heat at constant volume (c_v) and pressure (c_p).

3 Numerical implementation

To solve the one-dimensional NPE (Eq. 1), the operator splitting technique represents a versatile choice to solve sequentially and in a segregated fashion each term. It is based on the assumptions that all the terms are independent and that the time step is small enough [8]. The order in which the terms are solved is not relevant [17]. At the beginning of each time-step, the absorption term is solved with the Crank-Nicholson implicit scheme, a consolidated algorithm that provides unconditional numerical stability. This partial solution provides the initial field for the nonlinear term algorithm. Originally developed by *Boris et al.* [11], the Flux Corrected Transport method is designed to be second-order accurate, monotone, conservative and able to preserve positivity. It does so with two consecutive stages: the quantity is first convected and diffused, with the minimum amount of numerical diffusion required to prevent artificial oscillations and enforce positivity. Raw *anti-diffusive* fluxes are then computed and corrected in a second intra-step stage, by means of nonlinear flux-limiters intended to inhibit the generation of new local minima or maxima. The present work follows the formulation proposed by *Leissing* [4].

The initial acoustic pressure field is designed to match the experimental curve measured by the microphone located at 15 [m] from the muzzle (Fig. 1 – Left). The Friedlander wave model has been successfully used ([18], [19], [20]) to reproduce blast signatures of impulsive nature (overpressures), but repeated observations of large calibre weapons signatures highlighted the poor performance of the standard Friedlander model in matching the profile of the prominent and long lasting negative phase. A numerical waveform that inadequately represents the target experimental curve in time domain, will inevitably fall short in capturing the frequency content. Therefore, among the variants of the original Friedlander formulation, we selected one that stands out for its accuracy and does not depend on an empirical estimate of the explosive charge. It uses a cubic expression for the negative phase [20]:

$$p_r(t) = \begin{cases} p_{r,\max}\left(1 - \frac{t}{t_d}\right)e^{-b\frac{t}{t_d}} & t \le t_d \\ -p_{r,\min}\left(\frac{5.95(t - t_d)}{t_d^-}\right)\left(1 - \frac{(t - t_d)}{t_d^-}\right)^2 & t_d < t \le t_d + t_d^- \end{cases} \tag{4}$$

The semi-empirical piecewise definition allows to tune the positive and negative phase durations (t_d, t_d^-) and the absolute values of the positive and the negative peak amplitudes ($p_{r,max}$, $p_{r,min}$).

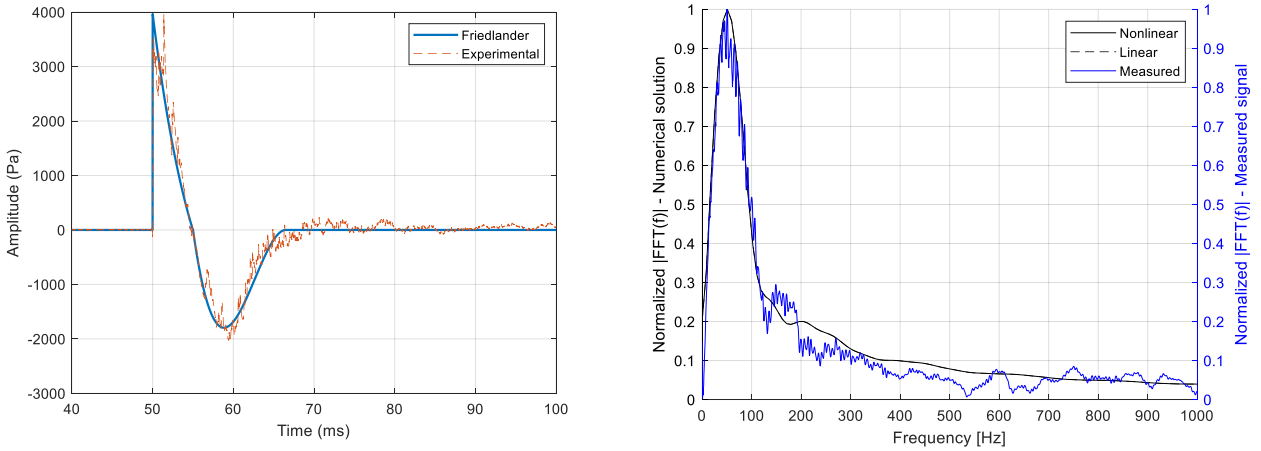

Figure 1 – *Left*: Time domain comparison of semi-empirical Friedlander model and measured signal at *x = 15 [m]*. *Right:* Single-sided spectra of the initial waveform

To avoid a loss of frequency content at the edges of the domain, the waveform is fully included in the window and surrounded by a sufficient number of wavelengths to account for leading and trailing quiescent intervals. Additionally, the length of the window must take into consideration the drift implied by the perturbation of the sound speed (*c'*). Multiplying the maximum expected sound speed by the propagation time provides an informed estimate of the distance travelled *within* the window [21]. It was found that a total length of L = 35 [m] satisfies both requirements. Given the number of spatial (N_x) and temporal points (N_t), the boundary conditions enforce the absence of perturbation sufficiently far from the shock:

$$R_0^n = R_{N_x}^n = 0 \ , \quad \forall \quad \mathrm{n} = 1, \ldots, \mathrm{N_t} \tag{5}$$

Steep pressure gradients and the shock formation make the grid's spatial resolution crucial. A common practice is to define the discretization based on a representative frequency. The signal under examination is broadband, with relevant frequencies ranging from 30 [Hz] to 8 [kHz]. It is conservative to assign 35 grid cells per characteristic wavelength, computed using the highest frequency of interest ($\Delta_x = 1.2 \cdot 10^{-3}$ $[m]$), whereas the temporal resolution is $\Delta_t = \frac{\Delta_x}{c_0} = 3.5 \cdot 10^{-6}$ $[s]$. The computational window advances of exactly one spatial grid point at each time step, providing numerical stability and making it straight forward and interpolation-free to post-process the results in the time domain.

3.1 Validation with analytical solution

Although no benchmark for the complete NPE equation is available, the mathematician Guido Fubini (1935) developed an analytical solution of the inviscid Burger equation [16]. Fubini's solution is valid for mono-frequency plane waves that propagate in a one-dimensional domain:

$$p(\sigma, \tau) = p_0 \sum_{n=1}^{\infty} \frac{2}{n\sigma} J_n(n\sigma) \sin(n\omega\tau) \tag{6}$$

with

$$\sigma = x / \bar{x}$$
$$\tau = t - x / c_0$$

$$\bar{x} = \frac{\rho_0 c_0^2}{\beta k P_0} = 64599[m]$$

No losses are included and its validity is limited up to the shock formation (σ = 1). As is done in [4] , the NPE benchmarking is done on a reduced version of Eq. (1), where only nonlinearity is taken into account:

$$\partial_t R = -\partial_x \left[\frac{\beta c_0 R^2}{2} \right] \tag{7}$$

Nonlinearity affects the propagation in a cumulative way. The positive peak of the sinusoid accelerates, while the trough decelerates. The shock, a mathematical discontinuity in the pressure field forming at $\bar{x}$, corresponds to a nearly infinitely steep curve in the discretized numerical domain, the characteristic N-shaped sawtooth wave (Fig. 2). The major implication is that the frequency spectrum undergoes a reshaping. The local increase in entropy caused by steepening acts as a dissipation mechanism that depletes the initial energy carried by the signal's principal harmonic and transfers it to a newly formed cascade of higher frequencies.

To verify that, a sinusoidal waveform of amplitude 1 [kPa] and frequency 0.1 [Hz] is propagated in air at ambient conditions with speed c_0. The chosen spatial resolution for the benchmark case is Δ_x = 0.0049 (m), corresponding to $\frac{\lambda}{100}$. The simulation ran for 66500 time-steps (Δ_t = 0.014 [s]), enough to propagate the sine-wave slightly beyond the shock formation distance.

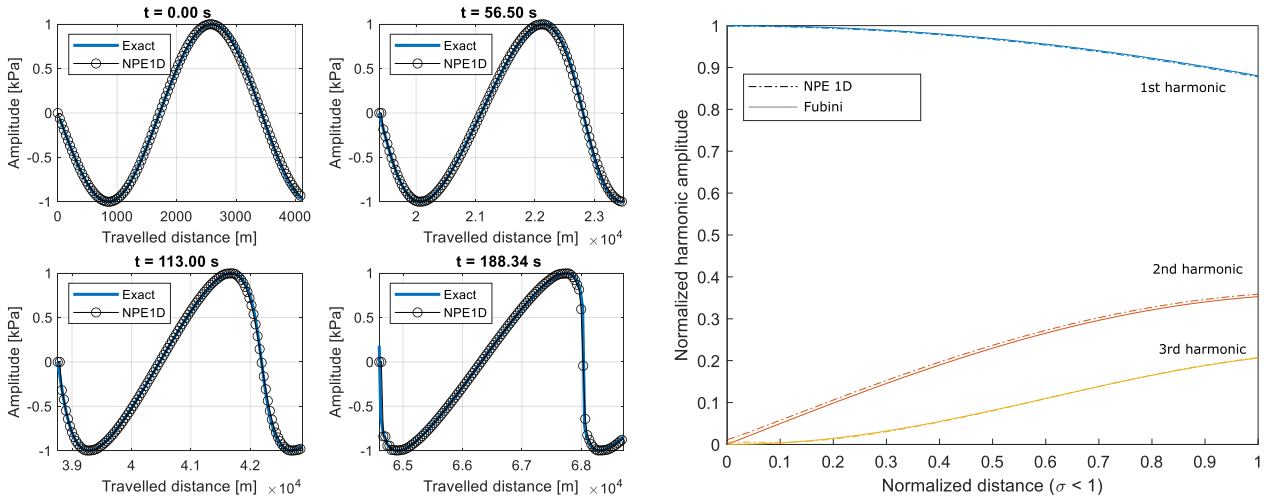

Figure 2 – *Left*: Comparison between the time-domain numerical solution for the plane inviscid Burgers equation and the theoretical Fubini solution [10] in the pre-shock region. *Right:* Evolution of the amplitude of the harmonics in the pre-shock region, normalized by the maximum initial value.

The steepening rate of the numerical solution in the time domain closely resembles that of the Fubini solution. The overestimation of the second harmonic takes the form of a constant offset, suggesting that the growth rate is not mispredicted. The gap rather originates due to a difference in the nature of the initial waveforms. The sinusoidal wave fed to the NPE solver is built analytically, while Fubini's solution at *t = 0 [s]* is a truncated Fourier series. Relative error metrics are not representative, because they disproportionately weigh the errors where the exact value is close to zero. The coefficient of determination (R^2) is a more appropriate absolute metric that assigns errors of *0.9962*, *0.9955* and *0.9994* respectively to the first, second and third harmonics. Ultimately, there is evidence that the implemented scheme closely reproduces the nonlinear effects of wave steepening while preserving the wave amplitude and its period.

4 Experimental setup

The test campaign's primary objective is to investigate the free-field propagation of weakly nonlinear waves radiating from the muzzle of a Howitzer 105 mm. The measurement system consists of four GRAS 46BG 1/4" pressure microphones (Frequency range: 3.15 Hz - 70 kHz, Dynamic range: 60 dB - 184 dB) and two GRAS 46AM 1/2" free-field microphones (Frequency range: 3.15 Hz – 31.5 kHz, Dynamic range: 25 dB - 49 dB). The sampling is performed at 70 [kHz] by two synchronized National Instruments modules (PXI-4462, PXI-4472) mounted on the same PXIe chassis. The recording of the data is triggered manually before every shot.

Table 1 – Atmospheric data

Quantity	Value
Ambient temperature	290.15 [K]
Atmospheric pressure	101250 [Pa]
Relative humidity	67.9 %
Wind	3.9 [m/s] (295°, W/NW)

The microphones are placed at a height of 1.5 [m] from the ground, as prescribed by [1] and [2] . Atmospheric conditions are monitored by a real-time operated weather station (Table 1) and averaged over the recording period. In order to mitigate the effect of wind and spurious background noise, each microphone is equipped with a foam windshield. The propagation path stretches along a grassy and mostly flat terrain, with occasional irregularities and dunes not exceeding 1m. The accurate modelling of the ground topography, even though essential, is beyond the scope of this work. Sources of uncertainty such as the receiver's position, the measurement chain and weather changes contribute to an extended measurement uncertainty $U_{k=1.96} = \pm 2.77$ dB (95% confidence interval).

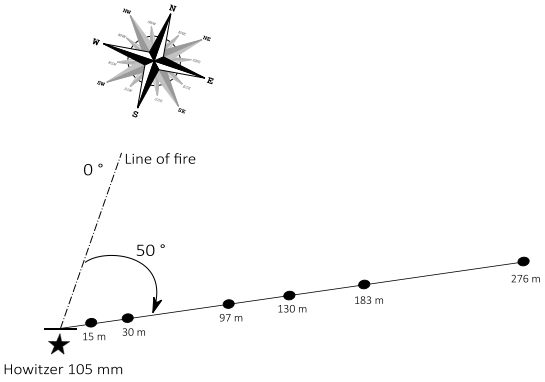

Figure 3 – Location of the microphones on the propagation line

5 Results

When quantifying the background disturbances, the spectra are averaged over three samples of 5 [s] each for the background noise, and three shots. Except for the 16 [kHz] cluster in Fig.2b, every frequency band is dominated by the shot's Sound Pressure Level by at least 10 [dB] [22]. The band-averaged 95% confidence intervals are shown in Fig.4 for the background noise and the Howitzer shot.

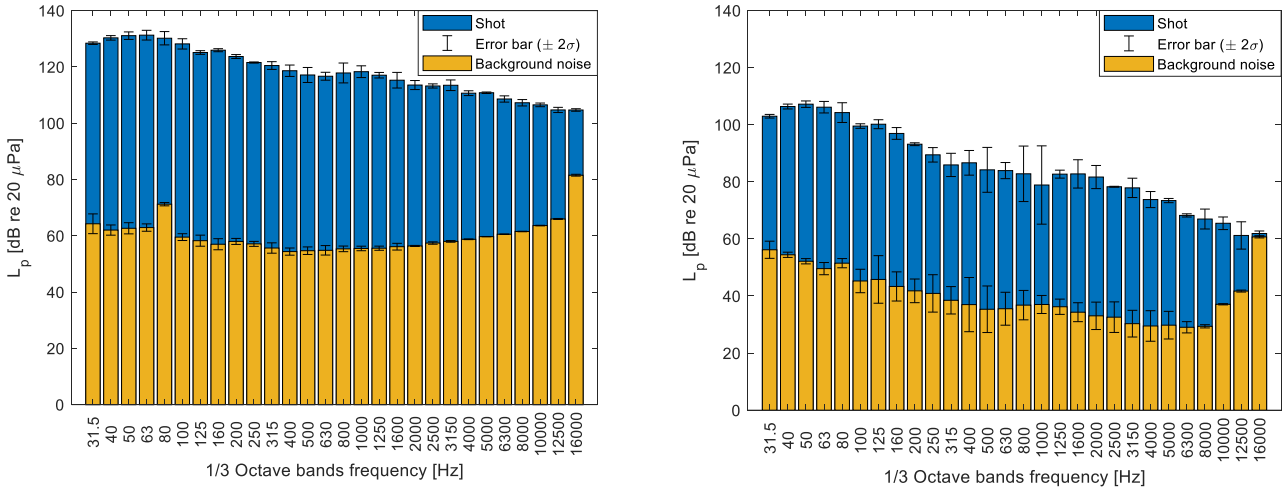

Figure 4 – Background noise quantification at (a) *15 [m]* and (b) *276 [m]* from the source

The time domain signal at each microphone location is cropped with a window length of 1 [s] to include the entire pulse (Fig. 1). The frequency domain counterpart is processed with one octave and 1/3 octave filter banks, to meet the standards' requirements ([1], [2], [3]). Given the sensitivity of the numerical solver to the initial conditions (Eq. 4), it was decided to select a single representative shot and investigate its propagation. This choice, although statistically sub-optimal, is motivated by the intention to preserve the tight link between one specific curve's time-domain parameters and its frequency content. Future work should certainly include more extensive statistical considerations. No directivity information is included in the framework, as only the 50° propagation path is under exam at this stage.

Table 3 summarizes each standard's approach to the calculation of the noise level at the receiver. The excess attenuation $A_e(r)$, computed similarly for each standard, includes ground effects, atmospheric absorption, geometrical divergence, barriers and diffraction. These quantities depend on the distance from the source r and the direction of the propagation line with respect to the line of fire α.

None of the standards is valid in the nonlinear range and for calibers larger than 20 [mm]. NT Acou 099 and ISO 9613 are based on the hypothesis that the acoustic event is continuous, neglecting the implications of the impulsive nature of a firearm shot.

Table 2 – Overview of the available standards

Standard	Receiver noise (dB)	Legend	Accuracy
ISO 17201 [1]	$L_E(r,\alpha) = L_q(\alpha) - A_e(r) + 11$	L_E: sound exposure level L_q : angular source energy distribution level	± 20 dB
ISO 9613 [2]	$L_{fT}(r,\alpha) = L_W + D_C(\alpha) - A_e(r)$	L_{fT} : equivalent continuous downwind sound pressure level L_W: sound power level D_c: directivity correction	± 3 dB
NT Acou 099 [3]	$L_{pI}(r,\alpha) = L_{pI}(\alpha, 10\,\mathrm{m}) + A_e(r)$	L_{pI}: time-weighted sound pressure level (I = 35 ms)	N.A.*

*Not specified by the standard, but a value of ± 3 dB can be assumed for the current configuration

Within A_e, spherical divergence is a dominant attenuation mechanism, being responsible for 6 dB of attenuation every doubling of the distance from the source [22]. Introducing an adjustment to the mono-dimensional NPE solution, although far from conclusive or rigorous, gives an educated estimate of the order of magnitude. The proposed correction [23] compensates for the spherical decay by multiplying the numerically obtained acoustic pressure field at each receiver's location by $\frac{r_0}{r}$. It derives directly from the geometrical observation that a

spherical plane wave departing from a point source carries an acoustic pressure perturbation that decays by *1/r* [22]. It is 1 when the receiver (*r*) is at the source position ($r_0 = 15$ *[m]).*

The linear solution ($\beta = 0$) with thermoviscous effects (*TH*) included is assumed as the baseline case. To illustrate the relative effects of nonlinearity (*NL*) and the divergence correction (*DIV*), these two propagation regimes are compared with experimental results and the standards' predicted values.

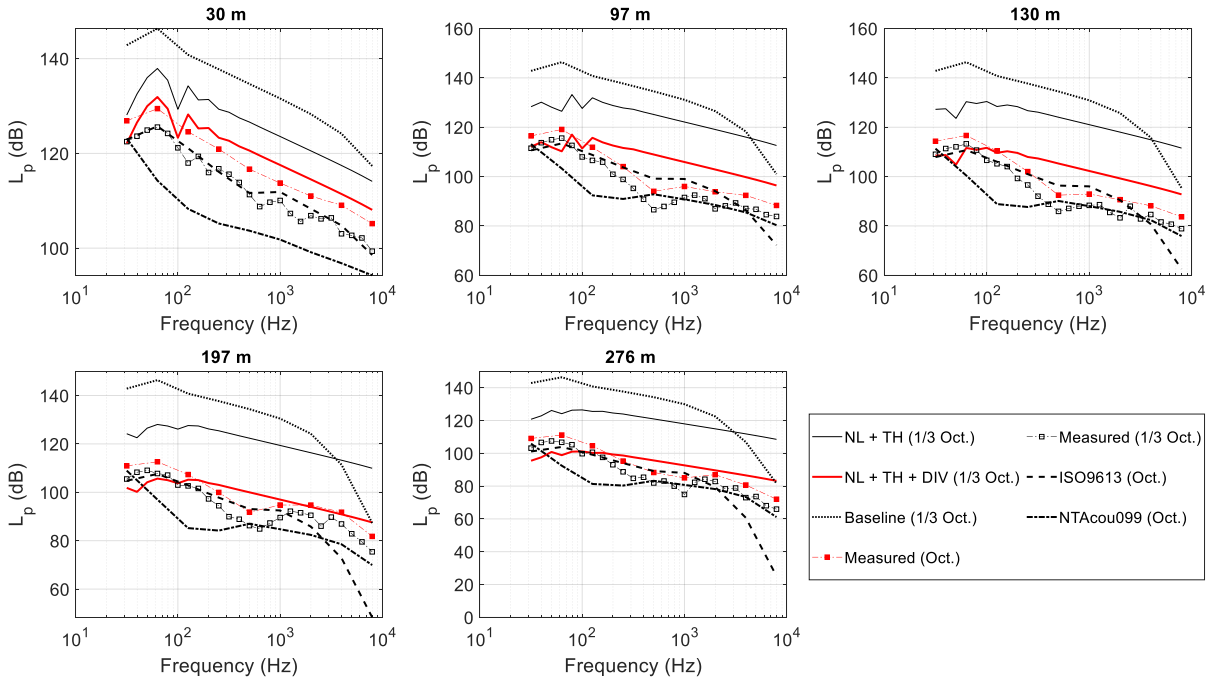

Figure 5 – Sound Pressure Levels, used in standards [2] and [3], at increasing distance from the Howitzer 105 mm

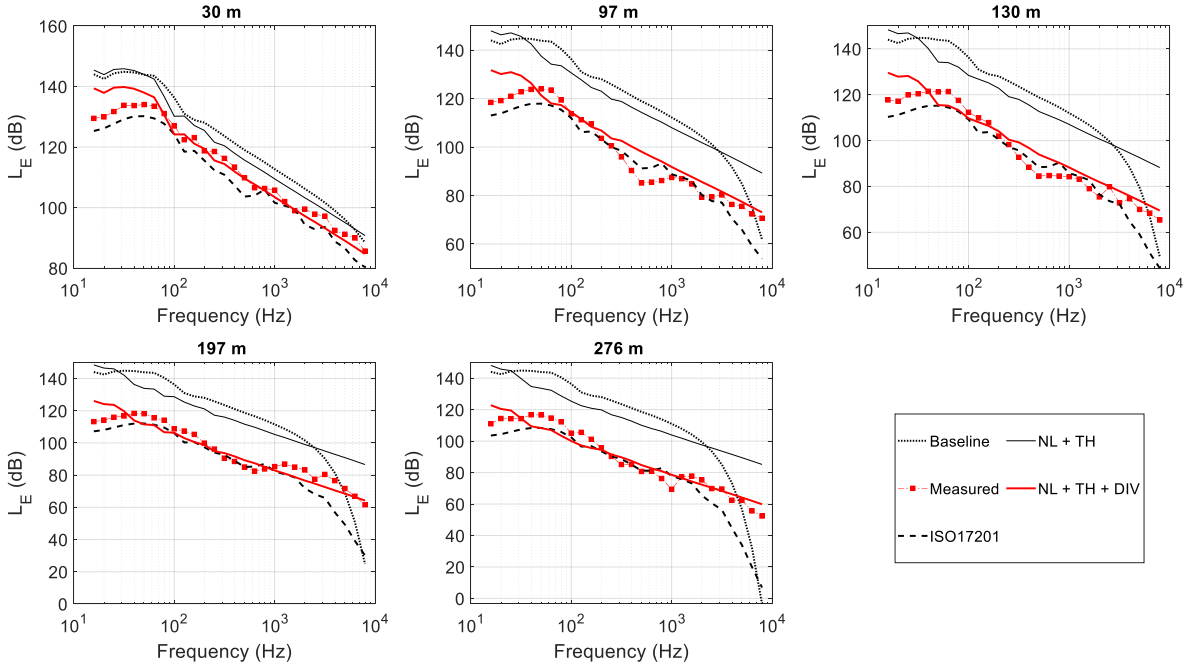

Figure 6 – Sound Exposure Levels, used in standard [1], at increasing distance from the Howitzer 105 mm

Except for NT Acou 099, the standards and the linear solution display a steep degradation of frequency content above 1000 [Hz] (Fig. 6 and Fig. 7a). The divergence-adjusted nonlinear solution outperforms both the ISO standards in matching the experimental values in the high frequency range. This behavior is consistent with the harmonics generation mechanism, absent in the linear domain and in the standards.

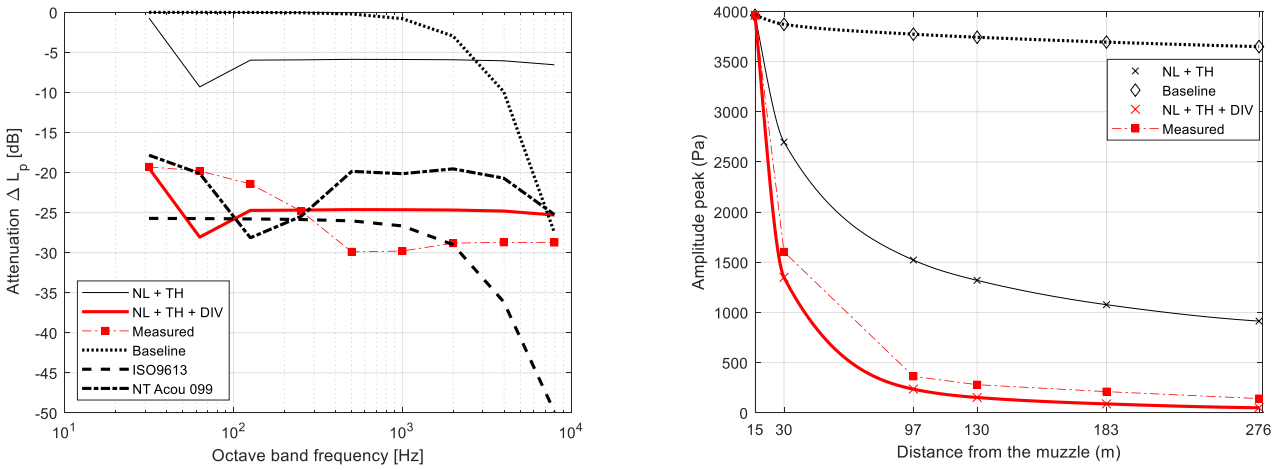

(a) (b)

Figure 7 – (a) Attenuation levels at *130 [m]*, relative to the signal at *15 [m]* and (b) decay of the maximum amplitude peak with distance

Fig. 7b shows that the nonlinear solution outperforms the linear one in reproducing the steep decline that occurs within the first 100 [m] of propagation. Adding the divergence attenuation to the mono-dimensional NPE solution inevitably overestimates the amplitude's decay (Fig. 7b) with respect to the measured values. If spherical divergence was embedded in a three-dimensional version of Eq. (1), the attenuation resulting from purely nonlinear effects would be smaller, as a consequence of the divergence-driven reduction of the peak dependent sound speed perturbation *c'* (Eq. 2) .

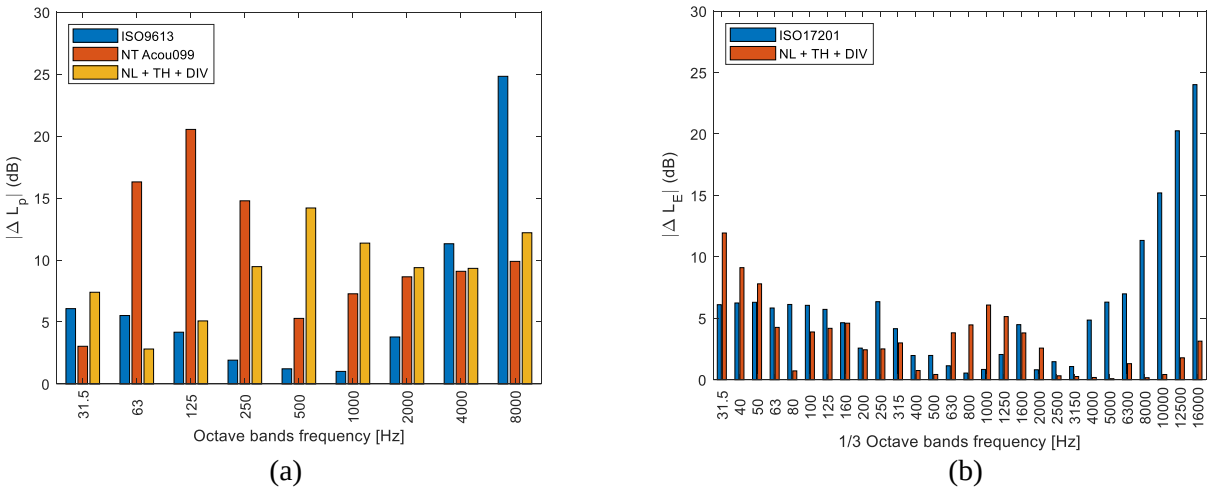

(a) (b)

Figure 8 – Absolute value of the difference between the experimental values and noise levels predicted by the NPE solution and the standards. Each frequency band is averaged over the five propagation distances.

As Fig. 8 displays, the numerical solution overall behaves better at higher frequencies and, unlike all three standards, never departs from the measured spectra of more than *15 [dB]*.

6 Conclusions

A weakly nonlinear pulse from a large caliber weapon was propagated for 261 [m] in air, using a one-dimensional solver for the Nonlinear Progressive Equation which accounts for non-linearities along the propagation as well as thermoviscous effects. A correction is implemented to account for spherical divergence. The solver is shown to behave adequately on Fubini's solution. The analysis of the measured and computed spectra confirmed the inadequacy of the present standards to accurately estimate the receiver noise over the entire frequency range, for a large caliber weapon for which no standard applies. When existing small and medium caliber standards are nevertheless applied, NT Acou 099 seems to perform best at frequencies higher than *500 [Hz]*, whereas the ISO standards better predict the spectrum in the *200 [Hz]* to *3000 [Hz]* range (Fig. 8). The capability of the nonlinear solver to closely predict the rate of amplitude decay (Fig. 7b), to provide good agreement with the experimental data in the high frequency range (Fig. 6 and Fig. 8b) and to limit the prediction errors to 15 [dB] (Fig.8) indicate a promising research direction. However, NPE's prediction of the low-mid frequency spectrum will be further improved including an upgrade to handle multi-dimensional phenomena such as spherical divergence, diffraction and ground effects.

Acknowledgements

The present work would not be possible without the scientific research funding of the Royal Higher Institute for Defence under grant MSP19/01. The authors wish to thank and acknowledge the contribution of the Artillery Battalion of the Belgian Defence, that made the Lombardsijde firing ranges accessible to us; the Material Evaluation Center of the Directorate General Material Resources; and of M. Van Cauter of the Royal Military Academy for his technical support.

7 References

[1] *Acoustics - Noise from shooting ranges - Part 1: Determination of muzzle blast by measurement (NBN EN ISO 17201-1:2019).*

[2] International Organization for Standardization [ISO], *Acoustics - Attenuation of sound during propagation outdoors - Part 1 : Calculation of the absorption,* 1996.

[3] Nordtest Method [NT], *Shooting Ranges : Prediction of Noise (NT Acou 099),* 2002.

[4] T. Leissing, "Nonlinear acoustic wave propagation in complex media : application to propagation over urban environments," 2009.

[5] S. M. Young, K. L. Gee, T. B. Neilsen and K. M. Leete, "Outdoor measurements of spherical acoustic shock decay," *The Journal of the Acoustical Society of America,* vol. 138, pp. EL305-EL310, 2015.

[6] K. Castor, P. Gerstoft, P. Roux and W. A. Kuperman, "Long-range propagation of finite-amplitude acoustic waves in an ocean waveguide," *Journal of the Acoustical Society of America,* vol. 116, pp. 2004-2010, 2004.

[7] B. E. McDonald and D. R. Plante, "Evidence for Self-Refraction in a Convergence Zone: NPE (Nonlinear Progressive Wave Equation) Model Results," 1989.

[8] Y.-S. Lee, "Numerical Solution of the KZK Equation for pulsed finite amplitude sound beams in thermoviscous fluids," 1993.

[9] M. Hajihasani, Y. Farjami, S. Gharibzadeh and J. Tavakkoli, "A novel numerical solution to the diffraction term in the KZK nonlinear wave equation," *38th Annual Symposium of the Ultrasonic Industry Association (UIA),* 2009.

[10] B. E. McDonald and W. A. Kuperman, "Time-domain solution of the parabolic equation including nonlinearity," *Computer & Mathematics with Applications,* vol. 11, pp. 843-851, 1985.

[11] J. P. Boris, A. M. Landsberg, E. S. Oran and J. H. Gardner, *LCPFCT - A Flux-Corrected Transport Algorithm for Solving Generalized Continuity Equations,* Washington DC: Laboratory for Computational Physics and Fluid Dynamics, U.S. Naval Research Laboratory, 1993.

[12] B. E. McDonald, "High-angle formulation for the nonlinear progressive-wave equation model," *Wave Motion,* vol. 31, pp. 165-171, 2000.

[13] B. E. McDonald, P. Caine and M. West, "A Tutorial on the Nonlinear Progressive Wave Equation (NPE) - Part 1," *Applied Acoustics,* vol. 43, pp. 159-167, 1994.

[14] P. Cainea and M. West, "A Tutorial on the Non-Linear Progressive Wave Equation (NPE). Part 2. Derivation of the Three-Dimensional Cartesian Version without Use of Perturbation Expansions," *Applied Acoustics,* vol. 45, pp. 155-165, 1995.

[15] B. O. Enflo and C. M. Hedberg, Theory of Nonlinear Acoustics in Fluids, vol. 67, S. S. &. B. Media, Ed., Kluwer Academic Publishers, 2006.

[16] A. D. Pierce, Acoustics - An Introduction to Its Physical Principles and Applications, Springer, Ed., ASA PRESS, 2019.

[17] J. Tavakkoli, D. Cathignol and R. Souchon, "Modeling of pulsed finite-amplitude focused sound beams in time domain," *The Journal of the Acoustic Society of America,* vol. 104, pp. 2061-2072, 1998.

[18] D. R. Glaser, M. J. White, D. K. Wilson and E. T. Nykaza, "Modeling of signal propagation and sensor performance for infrasound and blastnoise," in *Ground/Air Multisensor Interoperability, Integration, and Networking for Persistent ISR VIII,* 2017.

[19] J. R. Aguilar and S. V. Desai, "Model for Small Arms Fire Muzzle Blast Wave Propagation in Air," in *Unmanned/Unattended Sensors and Sensor Networks VIII*, 2011.

[20] S. Rigby, A. Tyas, T. Bennett and S. Clarke, "The Negative Phase of the Blast Load," *International Journal of Protective Structures,* 2014.

[21] T. Leissing, "Nonlinear outdoor sound propagation. A numerical implementation and study using the nonlinear progressive wave equation," 2006.

[22] J. R. Hassall and K. Zaveri, Acoustic Noise Measurements, Brüel & Kjær, 1979.

[23] P. V. Yuldashev, M. V. Averiyanov, V. A. Khokhlova, S. Ollivier and P. Blanc-Benon, "Nonlinear spherically divergent shock waves propagating in a relaxing medium," *Acoustical Physics,* vol. 54, pp. 32-41, 2008.